Chalcogenide Letters Vol. 22, No. 7, July 2025, p. 561 - 577

Structural, optical and electrical properties of NiO thin films for hole transport layer in chalcogenide and perovskite materials based solar cells

M. Abbas [a], M. Haseeb-u-Rehman [a], M. Sohail [b], G. H. Tariq [a,*]
[a] *Institute of Physics, Khawaja Fareed University of Engineering and Information Technology, Rahim Yar Khan (64200), Pakistan*
[b] *Department of Life Sciences, Khawaja Fareed University of Engineering and Information Technology, Rahim Yar Khan (64200), Pakistan*

This work presents the fabrication of NiO thin films via versatile sol-gel spin coating method and investigation of annealing effects on their physical properties. After the deposition process, the NiO thin films underwent annealing process at different values of temperatures ranging from 200°C to 350°C for one hour duration. XRD patterns confirmed the polycrystalline nature, along the preferred orientations (110) and (101) planes. Nanoparticles in NiO thin films demonstrated an increase in crystallite size with rising annealing temperatures, reaching a maximum size of 49 nm at annealing temperature 300°C. FTIR patterns revealed Ni-O bands at 472 cm^{-1} in the far infrared region. UV spectroscopy showed that the average transmittance of the NiO thin films increases 91% to 94% as a result of increasing the temperature during annealing. While the band gap decreases and reaches the lowest value 3.94 eV at 300°C. The hot probe tests of the fabricated nickel oxide thin films verified their p-type nature while the four-point probe technique showed that resistivity decreases at higher annealing temperatures. Based on these enhancements of physical properties, NiO thin films could be suggested as promising candidates for hole transport layer applications in chalcogenide and perovskite materials based solar cells.

(Received January 23, 2025; Accepted July 2, 2025)

Keywords: NiO thin films, Spin coating, Structural properties, Optical properties, Perovskite solar cells, p-type conductivity, Hole transport layers.

1. Introduction

One of the main problems that society is currently dealing with is the demand for sustainable energy. Only 85% of the world's energy needs are now satisfied by non-renewable fossil fuels, which have detrimental effects on the environment and human health. Solar power is a practical renewable power source that can contribute to supplying the world's energy needs. With little pollution, photovoltaic cells turn sunlight into electric power. Different materials are being studied for solar cell applications [1-4]**.** Over the past decade, scientists have made significant efforts to enhance the photovoltaic conversion efficiency (PCE) of perovskite solar cells (PSCs), increasing it from 3.8% to 25.7% [5]. PSCs are especially appealing due to their semiconductor qualities, which include their long electron and hole diffusion lengths, broad light absorption capabilities, and ambipolar transport facilitation [6]. When photons of light are absorbed by the perovskite layer, electrons from valance band are stimulated to the conduction band or lowest unoccupied molecular orbital (LUMO), which causes charge carriers to form in the material's bulk. Notably, perovskite has free electrons and holes instead of bound excitons because the latter's binding energy is enough to permit for charge separation at ambient temperature. The ambipolar conductivity of the perovskite materials causes the free positive holes and negative electrons to move through the material to the interface with the hole transport layer (HTL) or electron transport layer (ETL) respectively. In a typical perovskite solar cell, the level of the valance band or highest occupied molecular orbital of HTL is marginally greater than the perovskites. Furthermore, HTLs must meet some prerequisites, including: (a) HTL should have high mobility and carrier concentration (b) HTL should have a high band gap but the

* Corresponding author: g.hasnain@yahoo.com
https://doi.org/10.15251/CL.2025.227.561

HOMO energy levels of HTLs should match those of the perovskite layer (c) to prevent photon loss HTL should have high transmittance in the photoactive region (d) the HTL material shouldn't react with nearby components (e) HTL should have high thermal stability, (f) the HTL layers must have low defect concentration. This compatible criteria of selection of HTL material helps to reduce the charge recombination process by preventing the formation of holes at the interface and preventing the depletion of holes within the perovskite. Therefore, inverted perovskite solar cells (PVSCs) benefit from the HTL interface layer's increased charge-collecting efficiency, which raises PCE. So, the selection and engineering of p-type hole transport layer (HTL) in ABX_3 perovskite solar cells is very sensitive for enhancing their performance. Significant efforts are being made by scientists to research develop and optimize new p-type materials. For this purpose, many materials, such as CuO, CuSCN, CuI, MoS_2, WS_2, and NiO, are frequently used to fabricate a hole transport layer [7]. Among these materials, nickel oxide (NiO) stands out as one of the most versatile transition metal oxides and has a wide range of applications, including electrochromic devices [8], photovoltaic devices [9], chemical sensors [10], transparent electrodes in displays, solar cells [11], light-emitting diodes (LEDs) [12], lithium-ion batteries, and optical coatings [13]. Its versatility arises from many promising properties, including excellent cycle stability, high specific capacitance [14]. Due to their cubic p-type semiconducting nature, excellent transmittance, the wide band gap (E_g), ranging from 3.5 eV to 3.9 eV, high thermal stability, high surface area, and appropriate work function (WF) with deep valance band edge ranging from -5.2 eV to -5.4 eV that aligned with valance band of $MAPbI_3$ perovskite layer (-5.4 eV), NiO-based HTLs have been widely regarded as promising candidate in PVSCs [15]. Additionally, it is low cost, non-toxic and earth-abundant. Hence, it is very suitable to use NiO thin film as an HTL when deposited by a suitable technique.

Fabrication of thin films of metal oxides can be done using various methods, including spray pyrolysis [16-18], sputtering [19], electrochemical deposition [20], electron-beam deposition [21], pulsed laser deposition (PLD) [22], SILAR [23], chemical vapour deposition (CBD) [24], thermal deposition (TD) [25], and atomic layer deposition [26]. The sol-gel method is favoured because of its simplicity, versatility and cost-effectiveness. In contrast to other methods, it does not require too much pricey technological equipment. The spin coating technique includes four steps: (i) prepare a precursor solution [17]; (ii) age the precursor solution to turn it into a gel; (iii) coat sol-gel on a substrate; and (iv) dry and anneal thin films [27]. The characteristics of the films vary with several parameters, such as the ageing time, doping, concentration, spinning time, chelating agent, substrate temperature, post-heating temperature, annealing time, and spinning speed. Optimizing the ageing duration and heat-treatment parameters is highly important for fabricating nanoscale thin films by controlling optical bandgaps [28], among other aspects, to produce high-quality thin films. Many studies have looked at electrical, thermal, structural, chemical, optical, and electrochromic properties of NiO thin films. Both the annealing treatment and the deposition technique substantially affect the structural and optical characteristics of the deposited films. Few researches have explored the effects of annealing on physical characteristics, particularly employing the sol-gel spin coating approach [29, 30]. Therefore, this study investigates the effects of annealing on thin NiO thin films obtained via the sol-gel spin coating method to optimize the structural, optical, and electrical properties in order to determine the potential of NiO thin films as p-type HTL in PSCs.

2. Experimental work

2.1. Chemicals and substrates

A precursor material, nickel acetate tetra hydrated ($Ni(C_2H_3O_2)_2.4H_2O$, 98% purity), with CAS No. 6018-89-9, was acquired from Sigma Aldrich and used exactly as purchased to fabricate NiO thin films. A viscous liquid of 2-aminoethanol ($NH_2CH_2CH_2OH$ with purity >99.5%, CAS 141-43-5) was used as versatile liquid (solvent and as a stabilizer). Glass slides, cut nearly into square shapes with thicknesses of 1.2 mm (CAT No. 7101) were used as substrates.

2.2. Preparation of substrates

Well cleaned substrate is required for better adhesion of materials to be deposited on it. In the present work substrates were prepared for deposition by using a cleaning scheme in which a

series of three cleaning solutions; (i) a surfactant; first substrates were cleaned with lab cleaning surfactant, (ii) distilled water; in second step substrates were thoroughly cleaned in distilled water, and (iii) IPA for ten minutes each; in third and last step substrates were cleaned in IPA and then in IPA before shifting on substrate holder for deposition.

2.3. Deposition of pristine NiO thin films

The precursor $Ni(C_2H_3O_2)_2.4H_2O$ was successfully dissolved in 2-methoxyethanol to prepare the required solution. The nickel acetate concentration was held constant at 0.5 M. After one hour of homogeneous, transparent stirring at 50°C with a magnetic stirrer, the mixture was left to age for twenty-four hours at room temperature. The cleaned glass slides were then spin coated with this solution for 20s at 3000 rpm. To remove the organic residue, the prepared films were dried on a hot plate set at 100°C. Four layers were deposited on each substrate to prepare a thin film. All of the pure NiO thin films were then annealed from room temperature to 200°C, 250°C, 300°C, and 350°C using a 2.5 kW muffle furnace, which runs at 250V and has a rectangular cabin with an inner muffle dimension of 200 x 120 x 80 mm, ensuring regulated and consistent annealing.

2.4. Characterizations

Several characterization techniques, such as Fourier transform infrared spectroscopy (FTIR), ultraviolet (UV) spectroscopy, hot probe analysis, four-point probe measurements, and X-ray diffraction (BRUKER Germany), were used to examine their structural, optical, and electrical properties at different annealing levels. A simple, economical, and accurate mass difference technique was used to calculate the films' thickness [31-34]. It was found that the NiO thin films had an average thickness of 200 nm.

3. Results and analysis

3.1. XRD analysis

Structural changings induced in the NiO thin films after annealing were studied by XRD. The data was obtained for diffraction angles (2θ) ranging from 10 –70°. Fig. 1 shows the XRD results of NiO thin films which were annealed at 200, 250, 300, and 350 °C. The cubic-shaped, polycrystalline NiO thin films were oriented along the (110) and (101) planes at 30.34° and 27.7°. Typically, the preferential orientations for NiO nanoparticles attributed to annealed thin films were reported as (111) or (200) peaks but interestingly (110) NiO peak is found in this work and matches well with the NiO peaks of JCPDS card number 89-3980 [35], whereas the other weak peak oriented along (101) attributed to Ni_2O_3 (JCPDS card number 14-0481) is also found [36]. These XRD patterns were used to determine other structural parameters, such as full width at half maximum, dislocation density, crystallite size, and microstrain, which are summarized in Table 1.

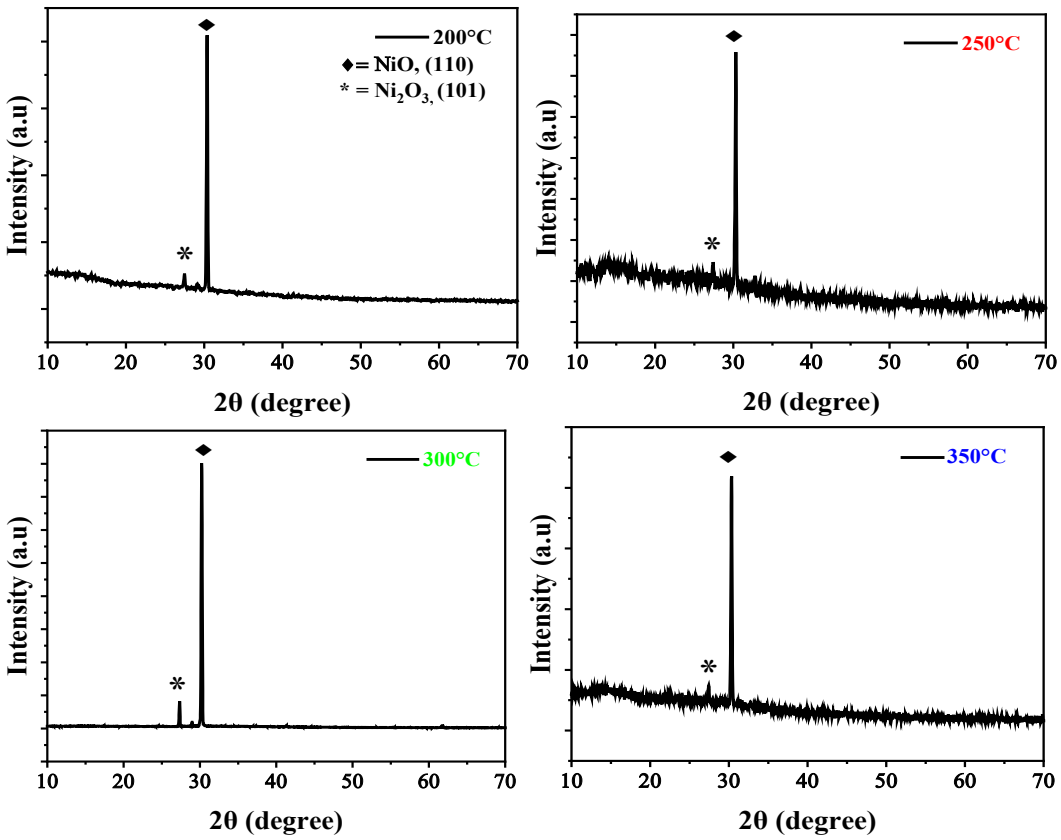

Fig. 1. XRD patterns of NiO thin films annealed at 200, 250, 300, and 350 °C.

The XRD data were also used to calculate the full width at half maximum (FWHM) by using origin software and then we calculated the crystalline size via Debye–Sherrer's relation [37].

$$D = \frac{k\lambda}{\beta cos\theta} \tag{1}$$

where usual names of factors "θ", "D", "k", "λ", and "β" are diffraction angle, crystallite size, shape factor, wavelength, and full width half maxima respectively. Williamson and Smallman's formula [38] was used for calculation the dislocation density [39, 40].

$$\delta = \frac{1}{D^2} \tag{2}$$

The factor "δ" denotes dislocation density and "D" cystallite size. The microstrain within the NiO thin films was computed via the following equation [40].

$$\varepsilon = {\beta cos\theta}/{4} \tag{3}$$

The micro strain "ε" scattering angle and FWHM are represented by "θ" and "β", respectively. Fig. 2 shows an increase in the crystallite size from 45.60 nm to 49.54 nm for annealing temperatures of 200 to 300°C, and then it decreases to 49.16 nm for an annealing temperature of 350°C. An overall increasing trend is observed for a specific range of annealing temperatures ranging from 200–350°C. One possible reason for the rise in crystallite size is the sintering process. At higher sintering temperatures, the rate of diffusion increases, which results in the promotion of the growth of crystallite size [41]. So, the increase in crystallite size found in this work may be attributed to the process of sintering [42]. The finding that NiO nanoparticles exhibit a large

crystallite size is not surprising. Arunodaya and Trilochan Sahoo reported a large crystallite size of 106 nm via the spin coating technique [43], while Ganesh et al. reported a crystallite size of approximately 53 nm using the same methodology. Fig. 2 also shows that micro strain decreases from 3.79×10^{-4} to 3.49×10^{-4} when annealing temperature jumps to 300°C and is in agreement with literature [44]. The highest crystallite size (49.54 nm) found in this work is distinctively smaller than the crystallite size reported [43]. The dislocation density decreases from $4.81\times 10^{14}/m^2$ to 4.07×10^{14} lines/m^2 with shifting temperature from 200 to 300°C, and then increases to 4.14×10^{14} lines/m^2 for 350°C and is in line with the research reported by Aswathy et al [14]. From these observations, it is evident that both the strain and dislocation density decrease, while crystallite size decreases, with increasing annealing temperature, indicating that annealing causes significant changes in structural properties of the NiO thin films. The rise in the crystallite size led to fewer defects and imperfections, indicating high thermal stability and good nanocrystalline structure [45]. All changes occurred in structural [39] parameters are in good agreement with many published reports [46, 47]. Normally good results are obtained by using thin films of moderately large crystallite size for fabrication of solar cells [48]. According to Prabeesh and his colleagues' findings, the thin films with the large crystallite size (47nm) exhibits higher carrier concentration of 4.12×10^{19} cm^{-3}, however thin film with the smallest crystallite size (11nm) had the lowest carrier concentration (6.62×10^{17} cm^{-3}). Hence, thin films prepared in this work having crystallite sizes 45 nm to 49 nm with additional features of being less defective and thermally stable show good potential to be used as HTLs in perovskite solar cells.

Table 1. FWHM, dislocation density, crystallite size, and strain of NiO thin films.

Temperature, T(°C)	Methodology	FWHM β(degree)	Crystallite size, D(nm)	Dislocation density δ(x10^{14}lines/m^2)	Micro strain, ε(10^{-4})
200	Sol-gel spin coating	0.18049	45.60	4.81	3.79
250	Sol-gel spin coating	0.17201	47.85	4.37	3.62
300	Sol-gel spin coating	0.16608	49.54	4.07	3.49
350	Sol-gel spin coating	0.16735	49.16	4.14	3.52

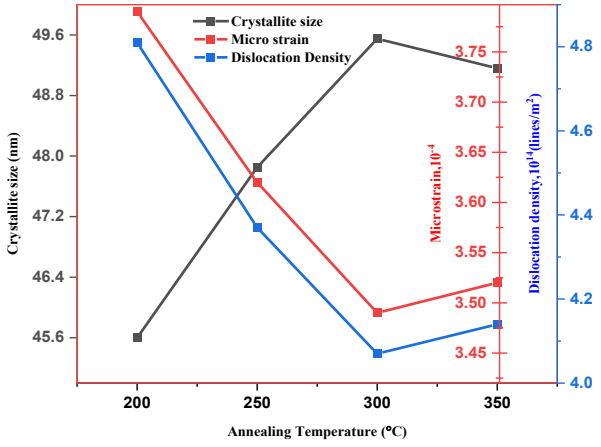

Fig. 2. Variations in the dislocation density, crystallite size, and strain of NiO thin films annealed at temperatures of 200, 250, 300, and 350°C.

3.2. FTIR analysis

FTIR spectroscopy is extensively employed to monitor microstructural evolution in response to processing parameters [49]. FTIR can also be used to reveal the formation of Ni–O bonds present in thin films treated at different annealing temperatures. Using this characterization, the annealing effects on the functional groups, intensities of the absorption bands, and vibrational modes were studied. Fig. 3 revealed that annealing alters the absorption bands broadening significantly. Stretching vibrations of hydroxyl (O-H) groups are typically detected in the spectral range 3000-4000 cm^{-1}, whereas O-H bendings are associated with a 1644 cm^{-1} band [50]. The NiO films developed a wide absorption band with a center at 3400 cm^{-1} after being annealed at 200°C. In the FTIR pattern of thin film annealed at 200°C, the broad absorption region of 2940-3860 cm^{-1} signifies the presence of O-H bands. The band centered approximately at 3400 cm^{-1} is associated with interlayer water (H_2O) molecules [51]. The characteristic $Ni(OH)_2$ band is at 3648 cm^{-1} [52]. The band centered at 2940 cm^{-1} links to C–H stretching while the band centered at 1644 cm^{-1} signifies absorbed moisture or the H-O-H group [53]. The absorption bands at 1409, 1339, and 1025 cm^{-1} correspond to various C-H and C-O modes resulting from the coating process [54] The bending at 676 cm^{-1} indicates hydroxyl groups where hydrogen is bonded to Ni-O.

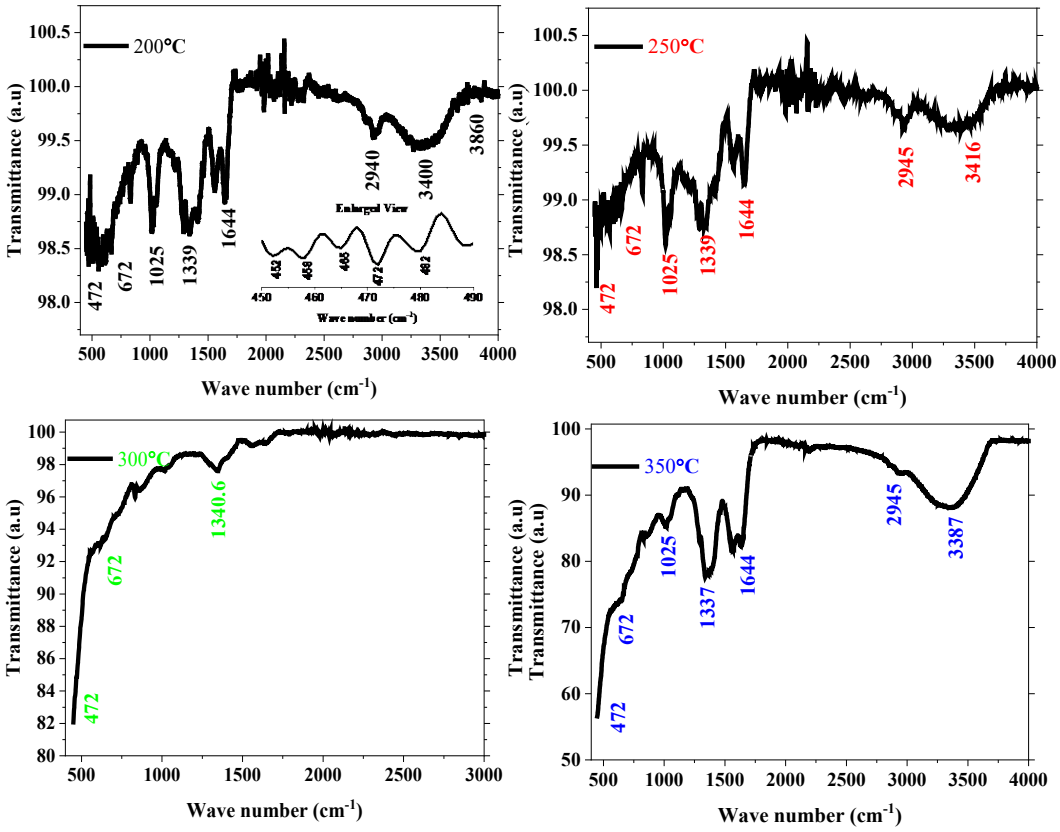

Fig. 3. FTIR patterns of NiO thin films annealed at different temperatures.

There is so much noise in region of 450 cm^{-1} to 4900 cm^{-1} but in an enlarged view of this region weak absorption lines associated with Ni–O bonding vibrations were observed and centered at 452, 458 and 472 cm^{-1} and are well aligned with reported research [44, 55-64]. A detailed comparison of the current work's findings with those of earlier Ni-O stretching investigations is provided in Table 2. In FTIR spectra of thin film annealed at 250°C the the bending at centered 472 cm^{-1} is much clearer than in thin film annealed at 200°C while 672 cm^{-1} band indicates hydroxyl group where hydrogen is bonded to Ni-O. A comparative FTIR analysis of all thin films revealed that the band attributed to $Ni(OH)_2$ is broader for thin film annealed at 250°C. Three bands, centered

at 472, 672, and 1339 cm^{-1} in the FTIR pattern of a thin annealed at 300°C, are ascribed to Ni-O, O-H, and C-O bonding, respectively. The narrowest bands are those at 672 and 1339 cm^{-1}. FTIR pattern of thin annealed at 350°C more or less shows the same bands mentioned in thin films annealed at 200°C, 250°C, and 300°C. Comparison of all patterns reveals that at low annealing temperatures (200 and 250°C), broader and stronger bands are observed, but their intensity decreases as the temperature increases to 300 and 350°C. A significant decrease in the broadening of O-H vibrations occurred due to the annealing process and O–H vibrations almost completely vanished for thin film treated at 300°C. Summarizing the FTIR findings, Ni-O bonding has been confirmed in all NiO thin films annealing renders NiO thin films OH-free, making these thin films good candidates for hole transportation in perovskite solar cells.

Table 2. FTIR band positions and assignments.

Band position (cm^{-1})	Assigned group stretching/bending	Reference
402, 415, 442	Ni-O	[59]
436	Ni-O	[57]
460	Ni-O	[58]
419, 614	Ni-O	[44]
461	Ni-O	[60]
550	Ni-O	[61]
500	Ni-O	[62]
435, 615	Ni-O	[63]
470, 522	Ni-O	[64]
475	Ni-O	[56]
452, 458 and 472	Ni-O	This work

3.3. UV–visible analysis

We employed UV-vis spectroscopy to collect the transmission data for NiO films in the region of 200–800 nm wavelength range of incoming light. The acquired transmission data were then utilized to determine critical optical parameters, including the absorption coefficient and band gap energy.

3.3.1. Optical transmission analysis

Each NiO thin film's transmittance spectrum is shown in Fig. 4. The annealing temperature has a significant impact on the optical transmittance of the NiO thin films. When the annealing temperature rises from 200 to 300°C, the transmittance rises from 91% to 94%, and when it reaches 350°C, it drops and reaches 89.6%. A significant decrease in the transmittance is observed approximately at 471 nm, 491 nm, and 521 nm for nanoparticles of thin films annealed at 200°C, 250°C, 300°C and 461 nm for those annealed at 350°C, respectively. A significant shift in transmittance to a higher wavelength [65] suggests that the predicted optical band gap values will decrease as by the increasing annealing temperature. and leading to the formation of good quality thin films. The improvement in transmittance is related to the enhancement in the microstructure, and results in less defect dispersion [47]. A less dispersive HTL minimizes variations in energy levels, leading to a smoother energy band alignment with the perovskite layer. This reduces energy losses during charge transfer and ensures consistent hole mobility, reducing the chances of charge trapping and recombination within the HTL [66]. Therefore, these less dispersive NiO thin films annealed at different temperature levels have the potential to be used in lasers, LEDs [14], and solar cells as p-type hole transport layers.

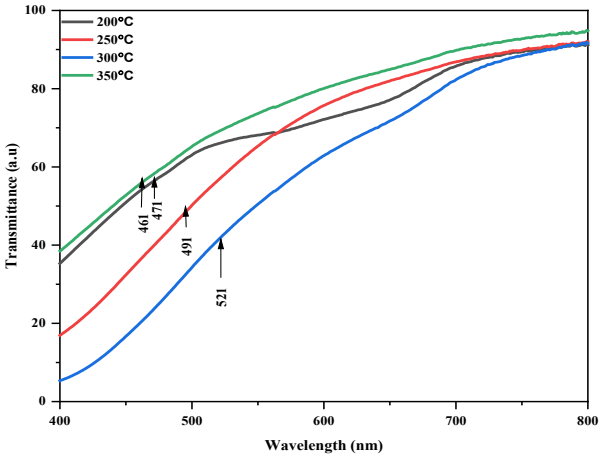

Fig. 4. Variation in the transmittance of NiO thin films versus wavelength.

3.3.2. Absorption coefficient

The ratio of the amount of light absorbed to the thickness of the film is called the absorption coefficient. Various materials absorb incident light differently across different energy ranges. The absorption coefficient was determined via a specific equation (4) called Lambert's law [67].

$$\alpha = -\frac{1}{t} lnT \tag{4}$$

"T" denotes the percentage transmission, whereas "t" denotes thickness of thin films. Fig. 5 shows a decrease in the absorption coefficient with increasing wavelength of incident light.

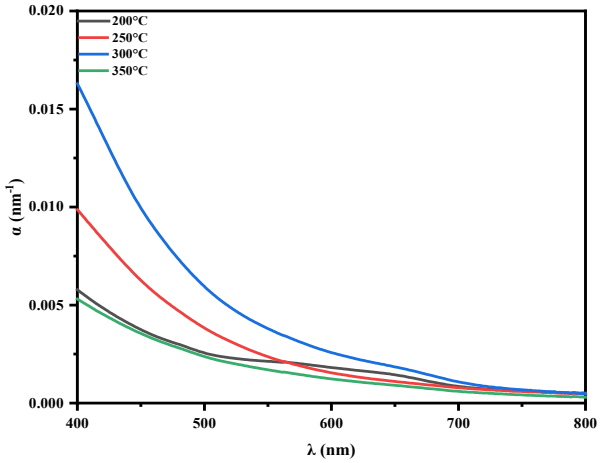

Fig. 5. Variation in the absorption coefficient of NiO thin films versus wavelength.

Fig. 5 shows that average value of the absorption coefficient increases from 0.0056 nm^{-1} to 0.0161 nm^{-1} as the temperature increases from 200°C to 300°C and finally it decreases when the annealing temperature further jumps and reaches 350°C. In this study, the energy-dependent absorption coefficients seemed to be greater in the visible light energy spectrum especially in the region of 400 nm to 450 nm and showing that prepared thin films allow more light to reach the perovskite layer. Therefore, these sol-gel-derived NiO thin films with such absorption coefficients can be used in solar cells. This pattern is consistent with findings from other research projects [68].

3.3.3. Band gap analysis

An electron needs energy to participate in the conduction process. The optical band gap energy (E_g) was determined via Tauc plots (Fig. 6) attributed to the following equation[69].

$$(\alpha h\upsilon)^{1/n} = \beta(h\upsilon - E_g) \quad (5)$$

The $\upsilon, \alpha, h, \beta$ symbolises frequency, absorption coefficient, Planck's constant and band tailing parameter respectively. The factor "n" frequently takes values such as 1/2, 3/2, 5/2, etc., or 2, 3, 4, etc., which correspond to direct and indirect band gap transitions while n is taken as 1/2 in this work. Tauc plots showed that the band gap values for thin films annealed at 200, 250, 300 and 350 are 4.01 eV, 3.99 eV, 3.94 eV and 3.97 eV respectively. The band gap decreased from 4.01 to 3.94 eV as the annealing temperature increased and is in good agreement of the literature [70, 71]. When the crystalline size increases, the sample band gap energy decreases due to the quantum confinement effect. The decrease in band gap reflects the decrease in number of defect sites [72, 73]. We observe that annealing lowers the band gap but it still is high as 3.99 eV. Perovskite materials' valence band and the highest occupied molecular orbital (HOMO) can be perfectly aligned by high bandgap hole transport layers (HTLs). This adjustment leads to efficient hole extraction, reduced resistive losses, and improved charge transport [74]. Hence annealing affects the optical properties NiO thin films to make them compatible with the perovskite layer.

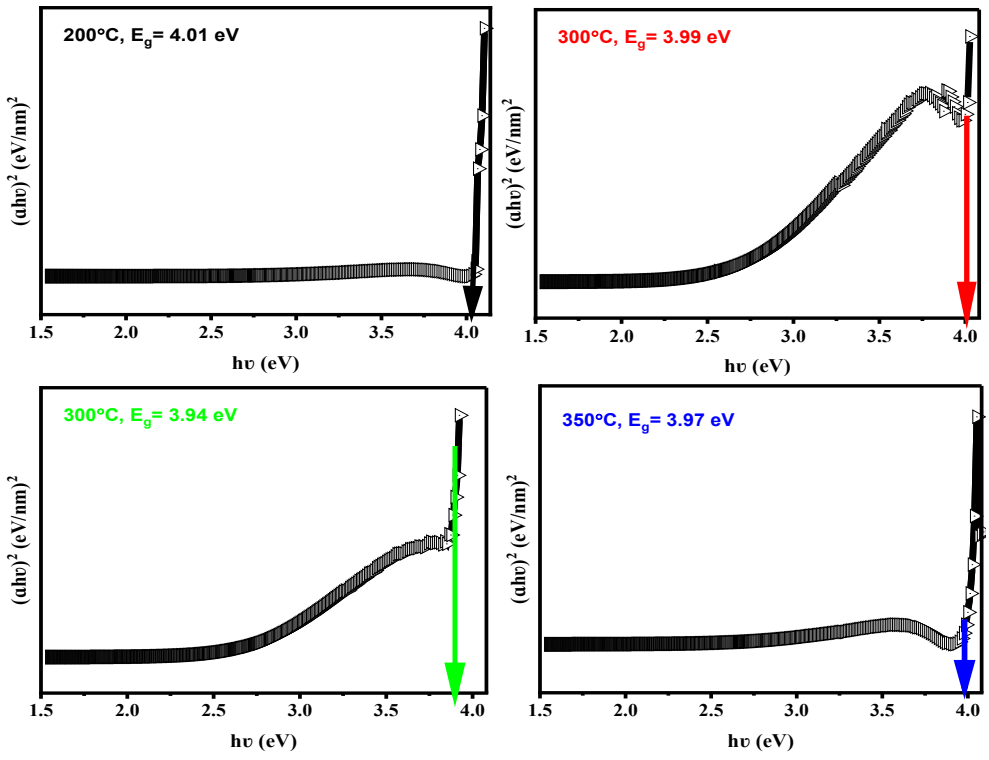

Fig. 6. Plots of $(\alpha h\upsilon)^2$ vs incident light energy ($h\upsilon$) for NiO annealed at different temperatures.

Table 3. Bandgap energies of NiO thin films for various annealing temperatures.

Deposition Methodology	Annealing temperature (°C)	Decreasing trend of band gap (eV)	Reference
Spin coating	300 – 600	3.75 – 3.50	[75]
Spin coating	000 – 500	3.72 – 2.98	[14]
Spin coating	300 – 600	3.83 – 3.66	[73]
Spin coating	300 – 700	3.86 – 3.47	[45]
Spin coating	350 – 600	3.75 – 3.66	[76]
Spin coating	200 – 300	4.03 – 3.94	This work
Spin coating	300 – 350	3.94 – 3.97	This work

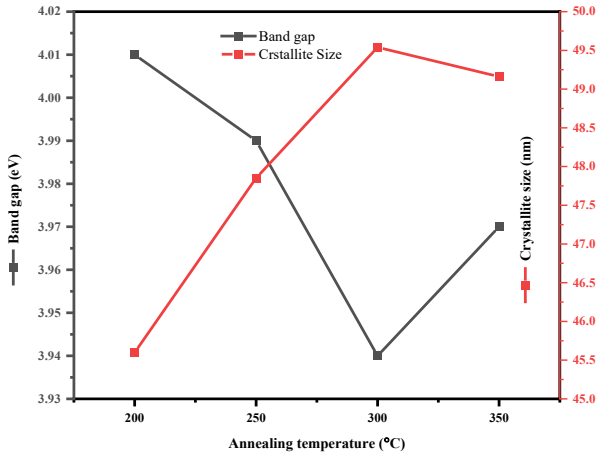

Fig. 7. Decreasing trend of the band gap with increasing annealing temperature.

Fig. 7 shows decrease in the band gap from 4.01 eV to 3.94 eV due to an increase with increasing temperature. The obtained values of bandgap energies of NiO thin films for various annealing temperatures are compared with literature as shown in Table 3.

3.4. Electrical analysis

3.4.1. Conductivity type determination

There are a number of methods for figuring out a semiconductor's conductivity, including wafer flat detection, electromotive force, rectification, the Hall effect, and a hot probe [77]. A straightforward, efficient, affordable, and precise hot probe approach is used in this work to examine the conductivity type for both n-type reference and p-type samples [78]. This method entails positioning two probes at various locations on the thin film's surface. By first heating the anode probe, a potential gradient is created between the two examining probes as electrons are forced to diffuse from the anode to the cathode (the cold probe). If the film being tested is n-type, a parallel-connected voltmeter detects the potential and displays a positive reading; if it is p-type, it displays a negative value. Fig. 8 **(**A) illustrates the negative conductivity of an n-type silicon wafer (reference) as measured by the hot probe method. The positive reading confirms that the reference film (the silicon wafer) exhibits n-type conductivity. In contrast, Fig. 8 (B) shows the response of the NiO thin film, which initially registers a negative response when heat is applied. A negative reading on the panel indicated that the sample exhibited p-type conductivity, and this response was consistent across all samples. The reaction intensified when heat was gradually applied above zero and diminished upon cooling [79]. As a result, the prepared samples are confirmed to be p-type materials. P-type conductivity ensures thin film has a holes' concentration and can be used as p type HTL. With a higher number of holes in the HTL, the material may easily enable the transfer of charge carriers, boosting overall device performance. In short, the p-type features of the HTL play an

important role in increasing electrical conductivity, resulting in improved device functioning and effectiveness. Hence these NiO thin films can be used in PSCs as p-type HTLs.

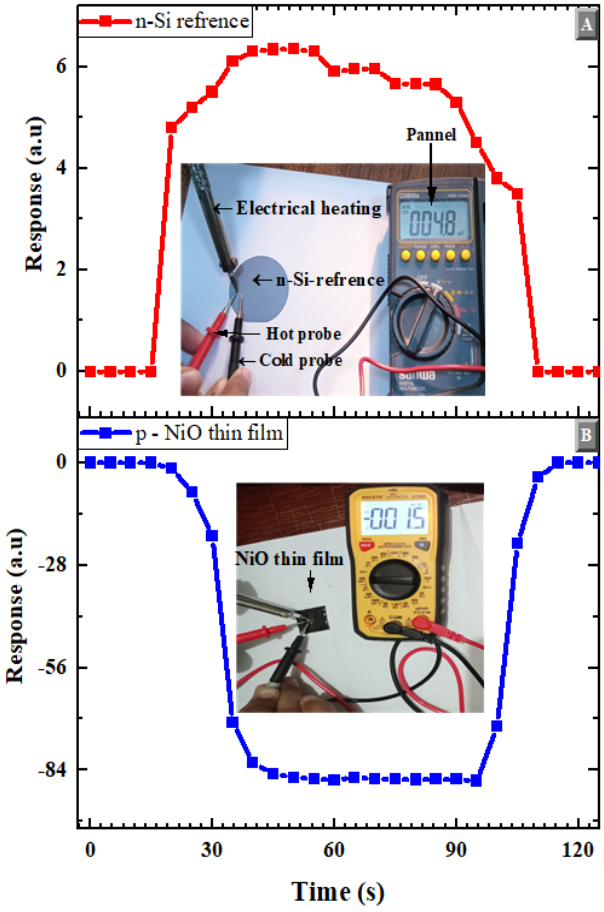

Fig. 8. Conductivity type measurement set-up: (A) n-type Si reference sample; (B) NiO thin film sample.

3.4.2. Resistivity measurement

There are many advantages for employing a four-point probe instead of a two-point probe to determine the sheet resistance (R) and resistivity (ρ). The four-point probe method is an easy, accurate, and low-cost approach that successfully overcomes the contact resistance problem, in contrast to the two-point probe leading to the more precise measurement of sheet resistance. A self-made local set up was made to determine the resistance of the thin films or sheets. It consists of a digital multimeter, a six-pin DC connector (out of six pins only four pins were used as probes), and an input current source. A 0.02 A current was passed through outer probes via an input current source, and then we observed the potential difference (V) between the inner probes on the display screen of the digital multimeter. Finally, we calculated the sheet resistance by using the data values in the following relation [80].

$$R = \left(\frac{\pi}{LN2}\right) \times \left(\frac{V}{I}\right) = 4.532 \left(\frac{V}{I}\right) \quad (6)$$

In the present measurement set-up, we used the probes with the 1.6 mm spacing which is higher than the thickness of thin film. So, we applied a correction factor of 4.532 in the above relation for square-shaped samples. The resistance values obtained from the relation were then used to find the resistivity by using relation given below [81].

$$\rho = Rt \tag{7}$$

Fig. 9 demonstrates that with the rise in annealing temperature (T) from its lowest value of 200℃ to 300℃, then the resistivity of the NiO films drops from its highest value of 2.04×10^{-5} Ω cm to 1.04×10^{-5} Ω cm , and finally, it increases up-to 1.22×10^{-5} Ω-cm at annealing temperature 350℃, showing the typical semiconducting behaviour [82].

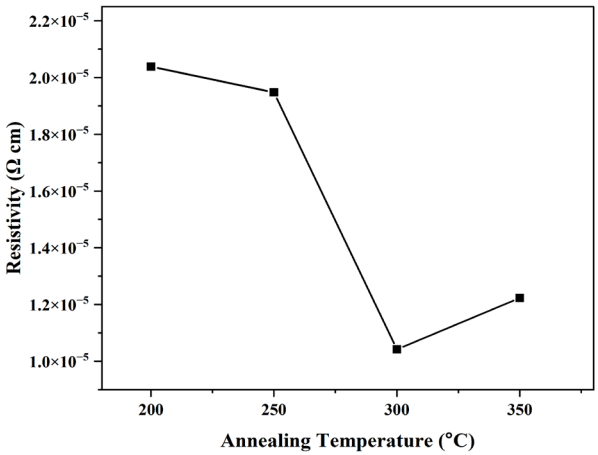

Fig. 9. Resistivity versus annealing temperature.

This decreasing and increasing trend of the resistivity may be attributed to the increase and decrease of crystallite size found in this work. The decrease in resistivity indicates an increase in the carrier concentration and mobility as resistivity varies inversely with them [83], which is necessary for creating an effective hole transport layer. The decreasing values 2.04×10^{-5} Ω cm to 1.04×10^{-5} Ω cm are very small than the resistivity values (24.70 Ω cm to 5.48×10^{-5} Ω cm) decreasing with annealing temperature reported in the previous literature [84]. The HTLs need to exhibit high conductivity and minimal resistivity. Low resistivity ensures that holes can move efficiently from the active layer to the electrode, enhancing device performance by reducing energy losses due to resistance [85]. Hence these low resistive NiO thin films show excellent potential to be used as hole transport layers for perovskite solar cell application.

4. Conclusion

In this research work, we employed a spin-coating deposition approach to fabricate NiO thin films. XRD revealed a polycrystalline nature with (110) as preferential orientations, with crystallite sizes ranging from 45.60 to 49.16 nm, which increased with increasing annealing temperature. FTIR findings revealed Ni-O stretching in the far infrared region at 472 cm^{-1} band position. We found a decrease in the band gap from 4.01 eV to 3.94 eV, and it finally increases to 3.97 eV. The optical investigations revealed temperature-dependent variations in the transmittance (91% to 94% then 94% to 89.6%), absorption coefficient (0.0056 nm^{-1} to 0.0161 nm^{-1} and then 0.0161 nm^{-1} to 0.0053 nm^{-1}), and optical band gap. The hot probe technique confirmed that NiO thin films had p-type conductivity. We can conclude that annealing enhances the optical and structural properties of NiO thin films fabricated via so gel spin coating technique. The key characteristics, such as large crystallite size, few defect sites, p-type conductivity, high band gap and low resistivity, make NiO thin films good candidates for use as hole transport layer applications in perovskite and chalcogenide materials based solar cells.

Authors' contribution

Conceptualization, G.H.T and M.A.; Methodology, G.H.T and M.A.; Formal analysis, G.H.T., M.A., and M.H.-u.-R.; Investigation, G.H.T., M.A; Data curation, G.H.T. and M.A.; Writing—original draft preparation, G.H.T. and M.A.; Writing-review and editing, G.H.T., M.A., and M.S.; Supervision, G.H.T.; Project administration, G.H.T. Funding acquisition, G.H.T. All authors have read and agreed to the published version of the manuscript.

Funding

The authors sought financial assistance through the Higher Education Commission (HEC) Pakistan, via project named as Punjab/NRPU/R&D/HEC/2017/10304.

Data availability statement

The article includes the original findings from the study; any additional questions should be addressed to the corresponding author.

Conflicts of interest

The authors declare no conflicts of interest. The funder played no role in the study's design, data collection, analysis, or interpretation, manuscript preparation, or decision to publish the findings.

Acknowledgements

The authors express their gratitude to the Higher Education Commission of Pakistan for providing financial support. through NRPU project named as Punjab/NRPU/R&D/HEC/2017/10304.

References

[1] S. Gao, J.J. Bae, D.S. Lee, T.Y. Yang, S.S. Shin, EcoMa, 7 (2025) 70001; https://doi.org/10.1002/eom2.70001

[2] I. M. Alarifi, Materials Today: Proceedings, 81 (2023) 403 -414; https://doi.org/10.20944/preprints202102.0345.v1

[3] M. Ochoa, S. Buecheler, A. N. Tiwari, R. Carron, Energy & Environmental Science 13 (2020) 2047-2055; https://doi.org/10.1039/D0EE00834F

[4] M. Tivanov, T. Razykov, K. Kuchkarov, A. Olimov, R. Khurramov, D. Isakov, Z. Makhmudov, M. Pirimmetov, A. Nasirov, D. Bayko, Journal of Applied Spectroscopy 91 (2025) 1249-1255; https://doi.org/10.1007/s10812-025-01845-w

[5] S. Khatoon, S.K. Yadav, V. Chakravorty, J. Singh, R.B. Singh, M.S. Hasnain, S.M. Hasnain, Materials Science for Energy Technologies, 6 (2023) 437-459; https://doi.org/10.1016/j.mset.2023.04.007

[6] S. Kazim, M.K. Nazeeruddin, M. Grätzel, S. Ahmad, Angewandte Chemie International Edition, 53 (2014) 2812-2824; https://doi.org/10.1002/anie.201308719

[7] S. Li, Y.-L. Cao, W.-H. Li, Z.-S. Bo, Rare Metals, 40 (2021) 2712-2729; https://doi.org/10.1007/s12598-020-01691-z

[8] H. Moulki, C. Faure, M. Mihelčič, A.Š. Vuk, F. Švegl, B. Orel, G. Campet, M. Alfredsson, A.V. Chadwick, D. Gianolio, Thin Solid Films, 553 (2014) 63-66; https://doi.org/10.1016/j.tsf.2013.10.154

[9] J.F. Wager, Science, 300 (2003) 1245-1246; https://doi.org/10.1126/science.1085276

[10] I. Hotovy, L. Spiess, M. Predanocy, V. Rehacek, J. Racko, Vacuum, 107 (2014) 129-131; https://doi.org/10.1016/j.vacuum.2014.04.012

[11] L. Cattin, B. Reguig, A. Khelil, M. Morsli, K. Benchouk, J. Bernede, Applied Surface Science, 254 (2008) 5814-5821; https://doi.org/10.1016/j.apsusc.2008.03.071

[12] J. Bandara, C. Divarathne, S. Nanayakkara, Solar Energy Materials and Solar Cells, 81 (2004) 429-437; https://doi.org/10.1016/j.solmat.2003.11.027

[13] L. Zhao, G. Su, W. Liu, L. Cao, J. Wang, Z. Dong, M. Song, Applied surface science, 257 (2011) 3974-3979; https://doi.org/10.1016/j.apsusc.2010.11.160

[14] N. Aswathy, J. Varghese, R. Vinodkumar, Journal of Materials Science: Materials in Electronics, 31 (2020) 16634-16648; https://doi.org/10.1007/s10854-020-04218-5

[15] G.M. Arumugam, S.K. Karunakaran, C. Liu, C. Zhang, F. Guo, S. Wu, Y. Mai, Nano Select, 2 (2021) 1081-1116; https://doi.org/10.1002/nano.202000200

[16] P. Raksa, W. Ponhan, E. Wongrat, A. Tubtimtae, Ceramics International, 51 (2025) 187861-8798; https://doi.org/10.1016/j.ceramint.2025.02.059

[17] M. Shkir, Journal of Sol-Gel Science and Technology, 113 (2025) 331-343; https://doi.org/10.1007/s10971-024-06622-3

[18] Y.M. Ashfaq, F. Yasmeen, I. Muneer, D. Ali, J. Farooq, S. Farid, Fuel, 390 (2025) 134703; https://doi.org/10.1016/j.fuel.2025.134703

[19] Y. Lu, W.-S. Hwang, J. Yang, Surface and Coatings Technology, 155 (2002) 231-235; https://doi.org/10.1016/S0257-8972(02)00037-3

[20] Y. Firat, Materials Science in Semiconductor Processing, 109 (2020) 104958; https://doi.org/10.1016/j.mssp.2020.104958

[21] O. Nakonechna, M. Dusheiko, N. Belyavina, A. Kuryliuk, A. Osipov, Metallofizika i Novejsie Tehnologii, 42 (2020); https://doi.org/10.15407/mfint.42.12.1659

[22] P. Misra, V. Sahu, R. Ajimsha, A. Das, B. Singh, Journal of Physics D: Applied Physics, 50 (2017) 415106; https://doi.org/10.1088/1361-6463/aa83ce

[23] O. Erken, Current Applied Physics, 34 (2022) 7-18; https://doi.org/10.1016/j.cap.2021.11.009

[24] L. N. Bhoye, L. D. Sonawane, A. S. Mandawade, S. S. Tayde, A. B. Gite, S. D. Shinde, G.E. Patil, V.H. Goswami, R.B. Bhise, P.B. Sarawade, M.S. Shinde, International Journal of Thin Films Science and Technology, 14 (2025) 111-117; http://dx.doi.org/10.18576/ijtfst/140206

[25] A. Chrissanthopoulos, S. Baskoutas, N. Bouropoulos, V. Dracopoulos, P. Poulopoulos, S. Yannopoulos, Photonics and Nanostructures-Fundamentals and Applications, 9 (2011) 132-139; https://doi.org/10.1016/j.photonics.2010.11.002

[26] M. Bonomo, Journal of Nanoparticle Research, 20 (2018) 222; https://doi.org/10.1007/s11051-018-4327-y

[27] H. Absike, H. Labrim, B. Hartiti, M. Tahri, H. Ez-Zahraouy, Molecular Crystals and Liquid Crystals, 711 (2020) 18-31; https://doi.org/10.1080/15421406.2020.1838065

[28] N. Touka, D. Tabli, K. Badari, Journal of Optoelectronics and Advanced Materials **21**(11-12), 698 (2019).

[29] S. Hadi, I. Khudayer, Chalcogenide Letters, 21 (2024) 885-893; https://doi.org/10.15251/CL.2024.2111.885

[30] G. Liu, G. Hu, P. Tang, L. Wu, X. Hao, G. Zeng, W. Wang, J. Zhang, Chalcogenide Letters, 21 (2024).

[31] A.A. Akl, A.S. Hassanien, Physica B: Condensed Matter, 620 (2021) 413267; https://doi.org/10.1016/j.physb.2021.413267

[32] M. Kul, Vacuum, 107 (2014) 213-218; https://doi.org/10.1016/j.vacuum.2014.02.005

[33] A.W. Faridi, M. Imran, G.H. Tariq, S. Ullah, S.F. Noor, S. Ansar, F. Sher, Industrial & Engineering Chemistry Research, 62 (2022) 4494-4502; https://doi.org/10.1021/acs.iecr.2c00416

[34] A.M. Koshy, A. Sudha, S.K. Yadav, P. Swaminathan, Physica B: Condensed Matter, 650 (2023) 414452; https://doi.org/10.1016/j.physb.2022.414452

[35] M.W. Alam, A. BaQais, T.A. Mir, I. Nahvi, N. Zaidi, A. Yasin, Scientific Reports, 13 (2023) 1328; https://doi.org/10.1038/s41598-023-28356-y

[36] I.R. Agool, M.K. Khalaf, S.H. Abd Muslim, R.N. Talaq, Engineering and Technology Journal, 33 (2015) 1082-1092; https://doi.org/10.30684/etj.2015.116476

[37] R. Kaliyaperumal, K. Nagaraj, K. Sakthikumar, M. F. Albeshr, G. Velmurugan, Applied Organometallic Chemistry, 39 (2025) 70121; https://doi.org/10.1002/aoc.70121

[38] A. Begum, A. Hussain, A. Rahman, Beilstein Journal of Nanotechnology, 3 (2012) 438-443; https://doi.org/10.3762/bjnano.3.50

[39] V. Ganesh, M. Shkir, M. Anis, S. AlFaify, Materials Research Express, 6 (2019) 086439; https://doi.org/10.1088/2053-1591/ab2090

[40] M.S. Hossain, S. Tarannum, M.A. Ullah, M.N. Uddin, N.M. Bahadur, S. Ahmed, International Journal of Applied Ceramic Technology, 22 (2025) 15025; https://doi.org/10.1111/ijac.15025

[41] L.K. Singh, A. Bhadauria, S. Jana, T. Laha, Acta Metallurgica Sinica (English Letters), 31 (2018) 1019-1030; https://doi.org/10.1007/s40195-018-0795-4

[42] S.-S. Liu, H. Li, W.-D. Xiao, Powder Technology, 273 (2015) 40-46; https://doi.org/10.1016/j.powtec.2014.12.016

[43] J. Arunodaya, T. Sahoo, Materials Research Express, 7 (2019) 016405; https://doi.org/10.1088/2053-1591/ab5bf1

[44] Z.N. Kayani, M.Z. Butt, S. Riaz, S. Naseem, Materials Science-Poland, 36 (2018) 547-552; https://doi.org/10.2478/msp-2018-0088

[45] P. Godse, R. Sakhare, S. Pawar, M. Chougule, S. Sen, P. Joshi, V.P. Patil, Journal of Surface Engineered Materials and Advanced Technology, 1 (2011) 35; https://doi.org/10.4236/jsemat.2011.12006

[46] B. Raut, S. Pawar, M. Chougule, S. Sen, V. Patil, Journal of alloys and compounds, 509 (2011) 9065-9070; https://doi.org/10.1016/j.jallcom.2011.06.029

[47] F. Hajakbari, M. Taheri Afzali, A. Hojabri, Acta Physica Polonica A, 131 (2017) 417-419; https://doi.org/10.12693/APhysPolA.131.417

[48] M.-S. Liang, Y.-K. Fong, C.-C. Khaw, C.-C. Liu, S.-P. Chin, Journal of Power and Energy Engineering, 2 (2014) 18-24; https://doi.org/10.4236/jpee.2014.212004

[49] P. Innocenzi, Journal of non-crystalline solids, 316 (2003) 309-319; https://doi.org/10.1016/S0022-3093(02)01637-X

[50] T. Ivanova, A. Harizanova, M. Shipochka, P. Vitanov, Materials, 15 (2022) 1742; https://doi.org/10.3390/ma15051742

[51] A. Kalam, A.S. Al-Shihri, A.G. Al-Sehemi, N. Awwad, G. Du, T. Ahmad, Superlattices and Microstructures, 55 (2013) 83-97; https://doi.org/10.1016/j.spmi.2012.11.024

[52] J. Kaspar, M.S. Bazarjani, C. Schitco, A. Gurlo, M. Graczyk-Zajac, R. Riedel, Journal of Materials Science, 52 (2017) 6498-6505; https://doi.org/10.1007/s10853-017-0885-0

[53] R.C. Korošec, P. Bukovec, Acta Chim. Slov, 53 (2006) 136-147.

[54] B. Govindarajan, R. Palanimuthu, K.M. Manikandan, Journal of Materials Science: Materials in Electronics, 30 (2019) 6519-6527; https://doi.org/10.1007/s10854-019-00957-2

[55] Y. Ghalmi, F. Habelhames, A. Sayah, A. Bahloul, B. Nessark, M. Shalabi, J.M. Nunzi, Ionics, 25 (2019) 6025-6033; https://doi.org/10.1007/s11581-019-03159-2

[56] A.J. Haider, R. Al-Anbari, H.M. Sami, M.J. Haider, Energy Procedia, 157 (2019) 1328-1342; https://doi.org/10.1016/j.egypro.2018.11.298

[57] S. Dewan, M. Tomar, R. Tandon, V. Gupta, c, Journal of Applied Physics, 121 (2017); https://doi.org/10.1063/1.4984580

[58] D.S. Hall, D.J. Lockwood, C. Bock, B.R. MacDougall, Proceedings of the Royal Society A: Mathematical, Physical and Engineering Sciences, 471 (2015) 20140792; https://doi.org/10.1098/rspa.2014.0792

[59] K. Purushothaman, S.J. Antony, G. Muralidharan, Solar Energy, 85 (2011) 978-984; https://doi.org/10.1016/j.solener.2011.02.012

[60] T. Taşköprü, E. Turan, M. Zor, International Journal of Hydrogen Energy, 41 (2016) 6965-6971; https://doi.org/10.1016/j.ijhydene.2015.12.008

[61] N. Srinivasa, K. Haunsbhavi, N. Srinatha, H. Mahesh, B. Angadi, Materials Today: Proceedings, 92 (2023) 1431-1437; https://doi.org/10.1016/j.matpr.2023.05.597

[62] R.C. Korošec, P. Bukovec, B. Pihlar, A.Š. Vuk, B. Orel, G. Dražič, Solid State Ionics, 165 (2003) 191-200; https://doi.org/10.1016/j.ssi.2003.08.032

[63] S. Benhamida, M. Gouamid, S. Tlili, A. Khenblouche, K. Charradi, Dig. J. Nanomater. Biostruct, 16 (2021) 433-442; https://doi.org/10.15251/DJNB.2021.162.433

[64] A. Rahdar, M. Aliahmad, Y. Azizi, NiO nanoparticles: synthesis and characterization, (2015).

[65] A.H. Hammad, M.S. Abdel-Wahab, S. Vattamkandathil, A.R. Ansari, Coatings, 9 (2019) 615; https://doi.org/10.3390/coatings9100615

[66] H. Taherianfard, G.-W. Kim, F. Ebadi, T. Abzieher, K. Choi, U.W. Paetzold, B.S. Richards, A. Alrhman Eliwi, F. Tajabadi, N. Taghavinia, ACS applied materials & interfaces, 11 (2019) 44802-44810; https://doi.org/10.1021/acsami.9b10828

[67] M.F. Hossain, M.S. Pervez, M. Nahid, Emerging Materials Research, 9 (2020) 186-191; https://doi.org/10.1680/jemmr.17.00085

[68] P. Sawicka-Chudy, M. Sibiński, G. Wisz, E. Rybak-Wilusz, M. Cholewa, Journal of Physics: Conference Series, IOP Publishing, 2018, pp. 012002; https://doi.org/10.1088/1742-6596/1033/1/012002

[69] N. Srinivasa, B. Angadi, H. Mahesh, Physics of the Solid State, 67 (2025) 598-605; https://doi.org/10.1134/S1063783425600311

[70] M. Martínez-Gil, M. Pintor-Monroy, M. Cota-Leal, D. Cabrera-German, A. Garzon-Fontecha, M. Quevedo-López, M. Sotelo-Lerma, Materials Science in Semiconductor Processing, 72 (2017) 37-45; https://doi.org/10.1016/j.mssp.2017.09.021

[71] T.Ç. Taşdemirci, Vacuum, 167 (2019) 189-194; https://doi.org/10.1016/j.vacuum.2019.05.047

[72] C.S. Garoufalis, A. Barnasas, A. Stamatelatos, V. Karoutsos, S. Grammatikopoulos, P. Poulopoulos, S. Baskoutas, Materials, 11 (2018) 949; https://doi.org/10.3390/ma11060949

[73] A.K. Srivastava, S. Thota, J. Kumar, Journal of Nanoscience and Nanotechnology, 8 (2008) 4111-4115; https://doi.org/10.1166/jnn.2008.AN36

[74] H. Bi, J. Liu, Z. Zhang, L. Wang, R. Beresneviciute, D. Tavgeniene, G. Kapil, C. Ding, A.K. Baranwal, S.R. Sahamir, ACS Energy Letters, 8 (2023) 3852-3859; https://doi.org/10.1021/acsenergylett.3c01275

[75] M. Jlassi, I. Sta, M. Hajji, H. Ezzaouia, Materials Science in Semiconductor Processing, 21 (2014) 7-13; https://doi.org/10.1016/j.mssp.2014.01.018

[76] P. Sahoo, R. Thangavel, AIP Publishing, 2018; https://doi.org/10.1063/1.5035243

[77] R. Wang, R. Moos, Journal of Materials Science, 56 (2021) 10449-10457; https://doi.org/10.1007/s10853-021-05949-4

[78] A. Axelevitch, Materials, 14 (2021) 1186; https://doi.org/10.3390/ma14051186

[79] G.H. Tariq, G. Asghar, M.S. Shifa, M. Anis-Ur-Rehman, S. Ullah, Z.A. Shah, I. Ziani, A.M. Tawfeek, F. Sher, Physical Chemistry Chemical Physics, 25 (2023) 31726-31740; https://doi.org/10.1039/D3CP04332K

[80] J.H. Kang, S.H. Lee, H. Ruh, K.M. Yu, Journal of Electrical Engineering & Technology, 16 (2021) 2265-2273; https://doi.org/10.1007/s42835-021-00725-5

[81] M. Naftaly, S. Das, J. Gallop, K. Pan, F. Alkhalil, D. Kariyapperuma, S. Constant, C. Ramsdale, L. Hao, Electronics, 10 (2021) 960; https://doi.org/10.3390/electronics10080960

[82] D.P. Joseph, M. Saravanan, B. Muthuraaman, P. Renugambal, S. Sambasivam, S.P. Raja, P. Maruthamuthu, C. Venkateswaran, Nanotechnology, 19 (2008) 485707; https://doi.org/10.1088/0957-4484/19/48/485707

[83] A. Qasrawi, N. Gasanly, Crystal Research and Technology, 36 (2001) 457-464; https://doi.org/10.1002/1521-4079(200106)36:4/5<457::AID-CRAT457>3.0.CO;2-I

[84] C. Park, J. Kim, K. Lee, S.K. Oh, H.J. Kang, N.S. Park, Applied Science and Convergence Technology, 24 (2015) 72-76; https://doi.org/10.5757/ASCT.2015.24.3.72

[85] S.T. Jan, M. Noman, Energy Technology, 11 (2023) 2300564; https://doi.org/10.1002/ente.202300564